View metadata, citation and similar papers at core.ac.uk

brought to you by CORE

provided by Elsevier - Publisher Connector

Pergamon

Available online at www.sciencedirect.com

SCIENCE DIRECT®

Acta Materialia 51 (2003) 4563–4574

Acta MATERIALIA

www.actamat-journals.com

Experimental determination of sintering stresses and sintering viscosities

Ruzhong Zuo *, Emil Aulbach, Jürgen Rödel

TU Darmstadt, Werkstoffe, FG Nichtmetallisch-Anorganische, FB 11 Petersenstr 23, Geb 73a, Darmstadt 64287, Germany

Received 21 February 2003; accepted 14 May 2003

Abstract

A loading dilatometer assisted by two high-resolution lasers was applied for the accurate measurement of radial and axial strains during uniaxial load assisted sintering. An improved hot forging technique was employed for the first time for the experimental determination of sintering stress and sintering viscosity by hot forging samples under various loads which were pre-sintered to different densities. The technique of discontinuous hot forging was discussed in detail and the effect of the developing anisotropy and different grain growth were analysed. The sintering stress and uniaxial viscosity were both obtained as functions of density ranging from 65 to 96% and compared with theoretical models. Alumina powder with a grain size of about 150 nm was used in this study.
© 2003 Acta Materialia Inc. Published by Elsevier Ltd. Open access under CC BY-NC-ND license.

Keywords: Sintering; Forging; Diffusion; Ceramics; Microstructure

1. Introduction

For cases where an externally applied compressive stress causes a linear increase in the corresponding densification strain, the viscoelastic analogue [1,2] can be used in combination with a well-known continuum mechanical formalism to describe complex sintering behaviour. This approach has the advantage that it can be used to predict the sintering behaviour of complex shapes [3], of cosintering layers [4,5] and thin films [6–8].

Theoretical descriptions [9–15] of sintering contain discussions on sintering stresses and sintering viscosities which are related to the dominating diffusion paths like grain boundary diffusion or lattice diffusion. A series of theoretical and experimental studies have applied this continuum approach to sintering problems [16–20].

The sintering stress and the uniaxial viscosity have repeatedly been investigated in both theoretical [9,12,13,21–24] and experimental aspects [18,19,25–27]. Different dependence on density was predicted, considering if grains grow or not.

Experimental approaches to the evaluation of these sintering parameters use a variety of techniques [25,28–33]. Amongst these, sinter forging is used as a common approach, where a uniaxial load is applied and radial and axial strains are measured [29,34,35]. The evaluation then relies on

* Corresponding author. Tel.: +49-6151-166312; fax: +1-49-6151-166314.

E-mail address: zuo@ceramics.tu-darmstadt.de (R. Zuo).

1359-6454/03 © 2003 Acta Materialia Inc. Published by Elsevier Ltd. Open access under CC BY-NC-ND license.
doi:10.1016/S1359-6454(03)00293-3

accurate determination of sintering strain rates, so that hot forging equipment for precise and concurrent measurement of radial and axial strains is required.

A common consideration on the experimental determination of continuum mechanical sintering parameters is that the density of the sample is used as only variable and that uniaxial loads will not affect the microstructure. The evaluation, however, is only valid if the microstructure as obtained by hot forging is identical to the microstructure as obtained by free sintering. In addition, this analysis assumes an isotropic microstructure. These conditions are explicit or implied assumptions in the analysis and require experimental verification.

Although the same approach was often adopted to determine these parameters as functions of density [18,19,36,37], little attention to microstructural change has been paid, particularly to pore orientation. This may have lead to conceptual errors involved in these analyses and experimental reports. Bordia, etc. [34,35,38] emphasised the importance of a microstructural verification in the experimental approach, yet few concrete experimental studies in this respect were reported. Our latest paper has critically evaluated the effect of uniaxial loads on the microstructure during hot forging [39]. We demonstrated that pores were elongated along the loading direction due to the application of a uniaxial compressive load during sintering and that anisotropic sintering behaviour was obtained. The anisotropy of microstructure was most efficiently assessed by employing free sintering studies on partially hot forged specimens. Similarly, Rahaman et al. demonstrated the anisotropy of free sintering after hot forging by comparing several strain rates at the same time [36,40]. In these cases, density is no more the only microstructural variable. Moreover, a difference in grain growth during hot forging and free sintering was considered to be another important microstructural bias, since grain size has a marked effect on sintering stress and viscosity. Therefore, a possible microstructural bias caused by uniaxial loads in hot forging experiments has challenged this experimental approach.

This study was initiated with the goal to resolve these problems by performing discontinuous hot forging. This is an improved hot forging technique where the sample is first allowed to sinter freely to prescribed densities, then the load is applied and the instantaneous radial and axial strains measured. We explore how this technique works and how the microstructure changes using this technique, as compared to continuous hot forging. The measured sintering stress and uniaxial viscosity were discussed using two microstructural factors: pore orientation and grain size. The results suggest that this technique is efficient in eliminating the microstructural bias in hot forging experiments under different uniaxial loads, and that the experimental determination in this study is valid.

2. Experimental

2.1. Hot forging apparatus and measurement

A new loading dilatometer was developed for hot forging experiments, which allows accurate determination of axial and radial strains during load assisted sintering [41]. This equipment mainly consists of a programmable heating furnace, a screw-driven loading frame and two high resolution laser scanners for the simultaneous measurement of radial and axial strains with a resolution of about 2 μm. The loading frame (Instron model 5565, max load 5 kN) has a fast response so that an accurately controllable uniaxial load (±0.1 N) can be applied on the specimen. An advantage of this loading system is that any specific load can be applied at any time (any density) during the whole period of sintering, so that it is ensured that different hot forging experiments can be started from the identical initial sample density. For the same reason, discontinuously loaded sintering experiments can be conducted.

An important element consists of an automatic positioning adjustment for the radial laser system. This design can greatly increase the accuracy of radial strain measurement because of the formation of concave (small loads) and convex (large loads) shapes which often exists during load assisted sintering. This system couples the position of the radial laser to the upper loading plate of the loading

train, such that the laser always measures the width of the specimen at its midpoint.

2.2. Materials

A commercially available Al_2O_3 powder (TM-DAR, Tokyo, Japan) with an average particle size of about 150 nm was used for this study. Cylindrical specimen were first pressed using an uniaxial pressure of 100 MPa and then further consolidated by cold isostatic pressing with 250 MPa. All final green cylindrical specimens are 20 mm in height and 11 mm in diameter, with a relative green density of 58.4 ± 0.2%. The samples are heated at a heating rate of 30 °C/min and held at 1250 °C for 2–4 h. As soon as the target temperature or the target density was reached, the loading system was activated for subsequent isothermal hot forging experiments. The load stabilises after a few seconds.

2.3. Measurement procedures

Discontinuous hot forging in this context implies that a uniaxial load was applied to pre-sintered samples. Data were then taken in a short time span after a uniaxial load was applied. Such experiments can be realised continuously from free sintering to load sintering at the target temperature as the loading system can be activated at any time. In this study, discontinuous hot forging runs were performed under uniaxial compressive loads of 50, 100, 150 and 200 N from densities of 65, 70, 75, 80 and 85% for each load. The above starting densities were realised by free sintering. At least 20 hot forging experiments were done, plus a complete free sintering experiment at the same temperature. For this study, the above densities corresponded to the free sintering strains of 3.41, 5.77, 7.91, 9.87 and 11.68% (engineering strains), respectively. They were used to determine the time when a uniaxial load will be activated, as these numbers are dynamically displayed on the computer monitor.

In order to assess how the microstructure changes during discontinuous hot forging, specimens were hot forged under 100 N load from the onset of isothermal sintering (the corresponding density of the sample is about 65%), from 70% density, from 75% density, from 80% density, and from 90% density up to several higher densities with a step of 5%. Once the required densities were reached, specimens were rapidly cooled for later microstructural investigation after the load had been released.

Next to the direct observation of microstructure, free sintering experiments of partially hot forged samples were performed. Specimens were hot forged intermittently from 65% density and 75% density, respectively, up to 80% density with 100 N uniaxial load, and then allowed to sinter freely by rapidly releasing the uniaxial load. This procedure affords assessment of the degree of anisotropy of sintering by comparing radial and axial strain rates [39].

2.4. Microstructural characterisation

Several cylindrical samples, as described above, were sliced in half from top to bottom. One piece of each sample was ground and polished to a 1 μm finish. The polished surfaces were then coated with a very thin carbon conductive layer for the examination of the pore morphology by high resolution scanning electron microscopy (HR-SEM, Model No. XL 30 FEG, Philips Electronic Instruments, Mahwah, NJ). Another piece of each sample was fractured and a small part of each sample was used for grain size measurement, applying a common linear intercept method with a factor of 1.466 on a series of SEM micrographs. This factor was determined by comparing the grain size measurement on the same samples with polished and fractured surfaces [42]. This is different from the common approach on a polished sample surface considering that thermal etching possibly causes grain growth and other microstructural changes (pore geometry and porosity), particularly for the samples with a rather low density.

3. Theoretical description

If a porous sintering body is assumed to be isotropic, the viscoelastic analogue can be used in combination with a well-known continuum mech-

anical formalism to describe the response of strain rates to stresses with the governing equations provided by Eq. (1a,b) in cylindrical co-ordinates

$$\dot{\varepsilon}_r = \dot{\varepsilon}_f + E_p^{-1}[\sigma_r - \nu_p(\sigma_\theta + \sigma_z)] \quad (1a)$$

$$\dot{\varepsilon}_z = \dot{\varepsilon}_f + E_p^{-1}[\sigma_z - \nu_p(\sigma_r + \sigma_\theta)] \quad (1b)$$

where E_p and ν_p are uniaxial viscosity and viscous Poisson's coefficient of a porous sintering body; $\dot{\varepsilon}_f$ is the free strain rate without externally applied stress; $\dot{\varepsilon}_r$ and $\dot{\varepsilon}_z$ are the radial and axial strain rates; σ_r, σ_θ and σ_z are the radial, hoop and axial stresses.

For uniaxial load assisted sintering of a cylindrical sample, the corresponding stress and strain state should be $\sigma_z \neq 0$, $\sigma_r = \sigma_\theta = 0$, $\dot{\varepsilon}_z \neq 0$ and $\dot{\varepsilon}_r \neq 0$. Thus, the Eq. (1b) can be further simplified to yield the following:

$$\dot{\varepsilon}_z = \dot{\varepsilon}_f + \frac{1}{E_p}\cdot\sigma_z \quad (2)$$

If the uniaxial viscosity E_p is only a function of density, the axial strain rate $\dot{\varepsilon}_z$ should obey a linear dependence on the external uniaxial stress σ_z.

Therefore, hot forging experiments were performed under different uniaxial stresses and the corresponding axial strain rates measured. A plot for axial strain rates $\dot{\varepsilon}_z$ vs. uniaxial stresses σ_z at a fixed density is shown in Fig. 1. The reciprocal of the slope of the straight line yields the uniaxial viscosity E_p at the corresponding density. On the other hand, the intercept $\dot{\varepsilon}_f \cdot E_p$ of this straight line with the stress coordinate provides the uniaxial sintering stress σ_s, as an external uniaxial tensile stress $\sigma_z = -\dot{\varepsilon}_f \cdot E_p (\dot{\varepsilon}_f < 0, E_p > 0)$ yields zero axial strain rate, as indicated in Eq. (2). Rearrangement of Eq. (2) gives:

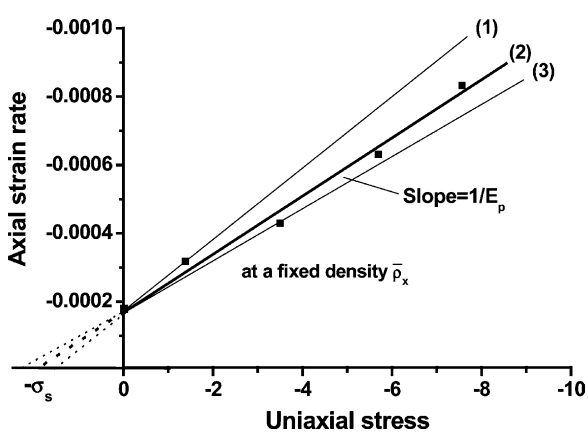

Fig. 1. A scheme of the response of axial strain rates to uniaxial stresses, describing the extrapolation method used to determine the sintering stress and the uniaxial viscosity.

$$E_p = \frac{\sigma_z}{\dot{\varepsilon}_z - \dot{\varepsilon}_f} \quad (3)$$

Eq. (3) indicates that the uniaxial viscosity E_p can be determined from one hot forging and one free sintering experiment. However, this tends to cause large errors in between Fig. 1(1) and (3). So the uniaxial viscosity E_p is preferably determined by performing hot forging experiments under several different uniaxial loads, as used in this study (Fig. 1(2)).

This extrapolation method has been used before to measure the sintering pressure in ceramic films [27], but no distinction was made between the uniaxial sintering stress $\sigma_s = \dot{\varepsilon}_f \cdot E_p$ and the hydrostatic sintering stress $\Sigma = \frac{\dot{\varepsilon}_f \cdot E_p}{1-2\nu_p}$. The definition of the uniaxial sintering stress σ_s follows the definition of uniaxial viscosity E_p and a one-dimensional strain rate $\dot{\varepsilon}_f$. In contrast, the hydrostatic sintering stress is related to the bulk viscosity K_p of a porous body and the volumetric strain rate $3\dot{\varepsilon}_f$, as indicated in Eq. (4),

$$\Sigma = 3\cdot K_p \cdot \dot{\varepsilon}_f = \frac{\dot{\varepsilon}_f \cdot E_p}{1-2\nu_p}. \quad (4)$$

In the experimental approach used in this study, an external uniaxial stress is applied so that the axial strain stops, but the radial shrinkage still continues, indicating a non-zero volumetric densification rate and the existence of shear deformation. It is apparent from Eq. (4) that the uniaxial sintering stress as determined in this study is smaller than the hydrostatic sintering stress. Determination of the uniaxial sintering stress σ_s only requires the free sintering strain rate $\dot{\varepsilon}_f$ and the uniaxial viscosity E_p. Measurement of the hydrostatic sintering stress requires also knowledge of the viscous Poisson's coefficient ν_p. Unfortunately, until now there are few reliable experimental data on ν_p, and conflicting theoretical descriptions [35], so that the experimental determination of the hydrostatic sintering stress Σ is rather difficult.

4. Results

4.1. Sintering strains during discontinuous hot forging

Five sets of hot forging experiments were conducted starting from several different densities. In each set, four different uniaxial compressive loads were employed and the corresponding strain vs. time curves were plotted. As an example, the hot forging run study with 70% density is provided in Fig. 2. The true strain definition was used, rather than engineering strains in the calculation of all sintering strains because of the large deformation involved in sintering. Before hot forging, specimens were sintered freely to the required densities at which a load was applied.

The sintering strain rates $\dot{\varepsilon}_r$ and $\dot{\varepsilon}_z$ of interest were then obtained by fitting exponential functions to curves of strain vs. time and taking their time derivative. Furthermore, considering the change of slope of the strain vs. time, different exponential functions were fitted to different parts of the curve. The quality of the fit was considered adequate when the absolute difference between fitted strain data and measured data by laser scanning was always within ±0.02%. This level of accuracy was considered sufficient as it is comparable to the experimental accuracy of the lasers used.

The instantaneous relative density of the samples during sintering can be calculated using Eq. (5),

$$\bar{\rho} = \frac{\rho_{gr}}{\rho_{th}\cdot\exp(2\varepsilon_r + \varepsilon_z)} \tag{5}$$

where $\bar{\rho}$ is the relative density of the samples at any time with respect to theoretical density ρ_{th}, ρ_{gr} the density of the green compacts. All curves in Fig. 2 can be then transformed into curves of strain rates vs. density. Only curves of axial strain rates vs. density were shown in Fig. 3 which were necessary for the following calculation.

4.2. Calculation of the uniaxial sintering stress σ_s and the viscosity E_p

Although a constant uniaxial load is always applied for each experiment, the applied stress changes due to the continuous radial strain. Therefore, instantaneous stress values during hot forging were calculated by considering instantaneous sample diameters (radial strains and original sample size).

Since in the following calculation the density of the sintered bodies is implied as an independent

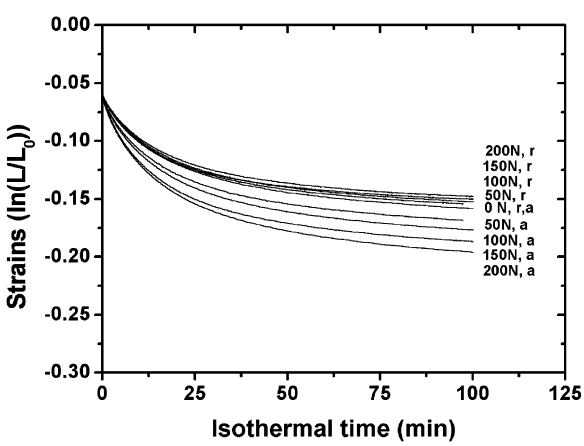

Fig. 2. True sintering strains: radial strain (*r*) and axial strain (*a*) with holding time during discontinuous hot forging experiments where uniaxial loads were applied from 70% density up to the end at 1250 °C. Before this density, all samples are freely sintered at the same temperature. Several constant uniaxial compressive loads were employed for each experiment, as indicated in the plot.

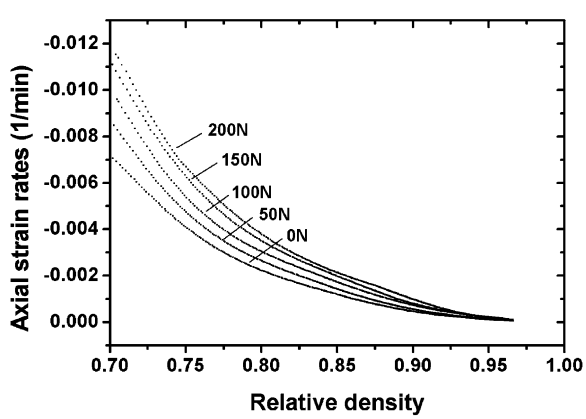

Fig. 3. Axial strain rates with density during discontinuous hot forging experiments where uniaxial loads were applied from 70% density up to the end at 1250 °C. For each experiment, different constant uniaxial compressive loads were employed as indicated. Before this density, all samples are freely sintered at the same temperature.

variable, the axial strain rates $\dot{\varepsilon}_z$ are presented at constant density as functions of the applied axial compressive stresses σ_z. Results are presented at different relative densities only for the experiment in which a load was applied from 70% density, as shown in Fig. 4. The results were linearly fitted, indicating that the axial strain rates $\dot{\varepsilon}_z$ have a linear relationship with the uniaxial stresses σ_z, which is identical to the theoretical description from Eq. (2) by assuming that the uniaxial viscosity is only a function of density. In Fig. 4, the results were shown only at select densities. Note, however, that the above-mentioned linear curves of $\dot{\varepsilon}_z$ vs. σ_z can be obtained at any density.

From each straight line in Fig. 4, the sintering stress σ_s as well as the uniaxial viscosity E_p at a fixed density can be computed (Fig. 1). The results for both sintering parameters as a function of density are provided in Figs. 5 and 6, respectively. All data denoted by different signs in Figs. 5 and 6, correspond to experiments that started at different densities. For each set of experiment, for example, applying loads from 65% density, the data only within the range of density of a few percent (about 5%) after a load was applied, are useful, as a possible microstructural bias is enhanced with time by the uniaxial load. The envelope from the different sets of experiments was then plotted in a wider density range (Figs. 7 and 8). It is clearly seen from Figs. 5 and 6 that the microstructural bias, as discussed previously, has an apparent effect on the experimental determination of the sintering stress and the uniaxial viscosity. Taking a density of 90% as an example, a possible microstructural change led to the determination of a smaller absolute sintering stress (Fig. 5) and a lower uniaxial viscosity (Fig. 6) when a load was applied from 65% density, as compared to those when a load was applied from 85% density. The longer the uniaxial load was applied, the stronger the possible microstructural change and the lower sintering stress and viscosity are determined using this approach. Clearly,

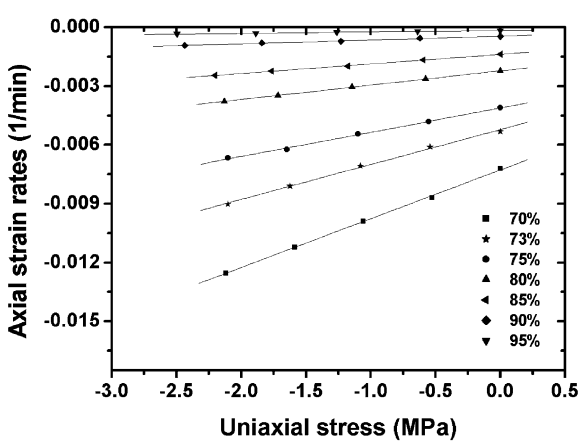

Fig. 4. Axial strain rates as a function of uniaxial compressive stresses at constant density as indicated for experiments where several loads were applied from 70% density up to the end.

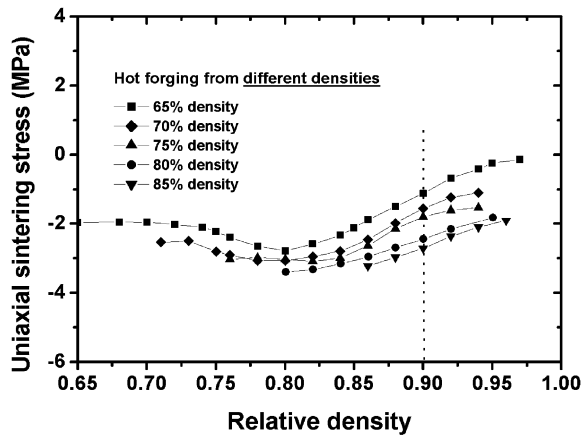

Fig. 5. Sintering stresses as a function of density as derived from several discontinuous hot forging experiments.

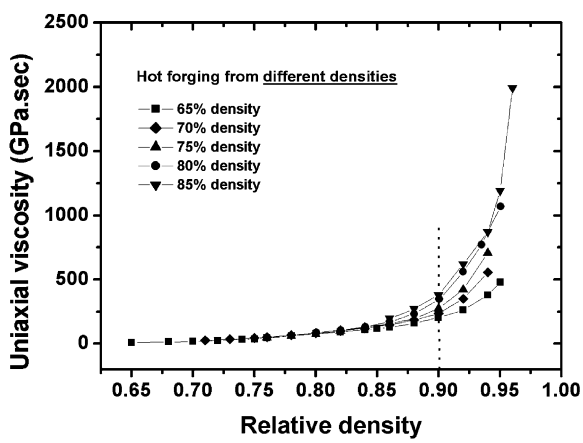

Fig. 6. Uniaxial viscosity as a function of density as obtained from several discontinuous hot forging experiments.

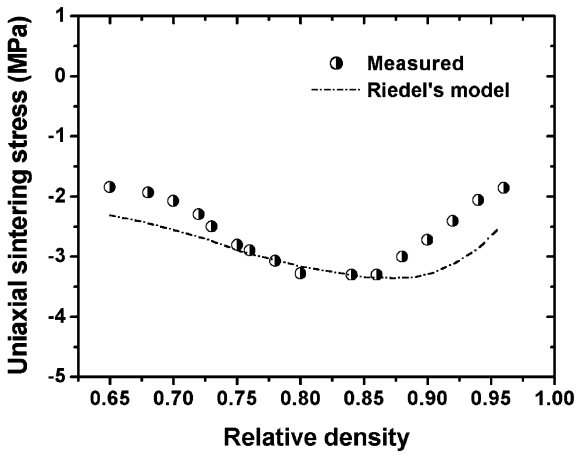

Fig. 7. Sintering stress as a function of density derived as the envelope from several discontinuous hot forging experiments as indicated in Fig. 5.

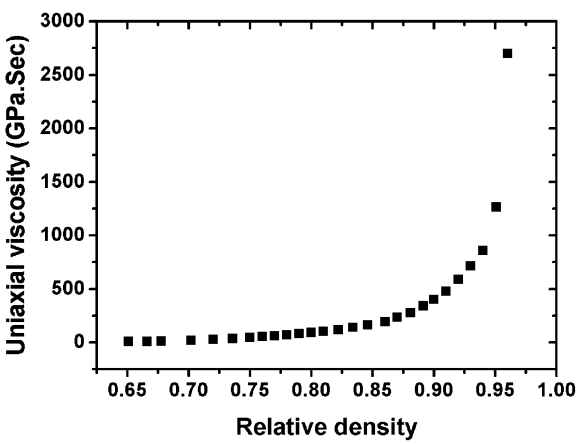

Fig. 8. Uniaxial viscosity as a function of density obtained from the envelope to the curves in Fig. 6.

this effect has been greatly improved by using the data from discontinuous hot forging experiments.

4.3. Microstructures of discontinuously hot forged samples

As mentioned above, isotropy of microstructure during hot forging and identical microstructure (grain size and shape, pore orientation and geometry, etc.) between freely sintered samples and hot forged samples at the same density, have to be guaranteed. As shown in Fig. 2, the freely sintered sample under 0 N uniaxial load presents almost completely identical strain vs. time curves in radial and axial directions, indicating isotropic free sintering behaviour. In spite of this, the microstructural verification needs to be provided for hot forged samples.

Grain size was first measured for samples obtained by different sintering processes, as indicated in Fig. 9. The grain sizes of freely sintered samples are larger than those of hot forged samples at the same density and the difference tends to increase with time. Moreover, the sample hot forged from a lower density, may have a smaller grain size. At the density of 95%, a freely sintered sample has a much larger grain size than the sample hot forged under 100 N load starting from 70% density. The difference is demonstrated in Fig. 10. The explanation for this change is that grain growth is mainly a function of time, initial grain size and temperature, and that a uniaxial compressive load may shorten the time for which the same density can be reached, as compared to free sintering. Nevertheless, no preferred grain growth orientation was observed in this study. In contrast, a freely sintered sample has almost the same grain size at 95% density, as another sample hot forged under 100 N load from 90% and even from 80% density. The result verifies that the same grain size

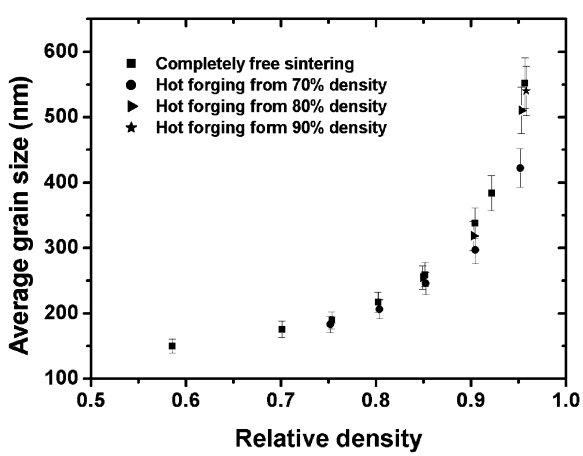

Fig. 9. Grain sizes of samples from free sintering and discontinuous hot forging under 100 N uniaxial load from different starting densities up to higher densities. When the required density was reached, the heating was stopped at once.

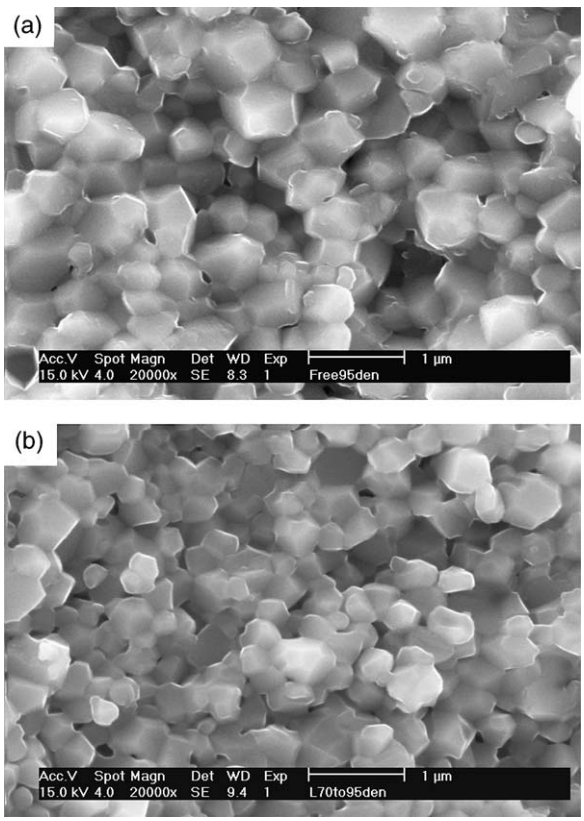

Fig. 10. SEM photos showing different grain sizes of the samples with the same density of 95% by (a) free sintering and (b) hot forging under 100 N load starting from 70% density.

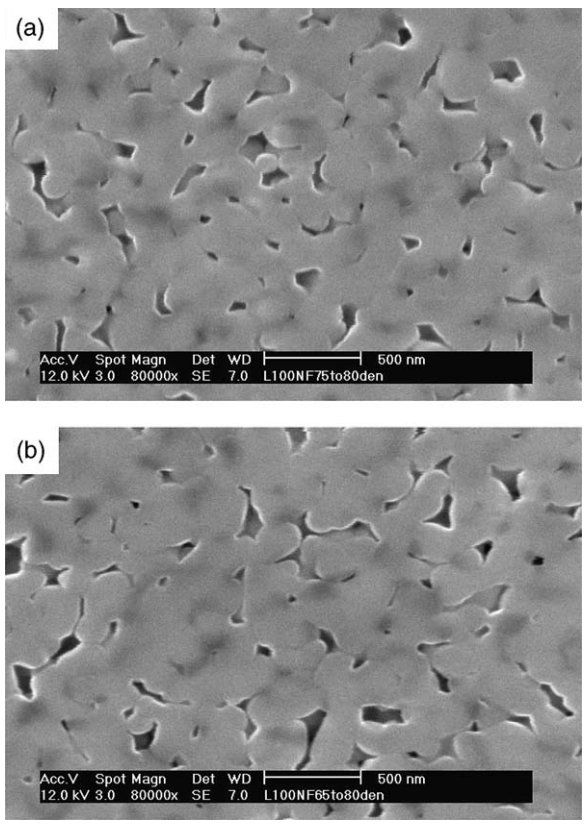

Fig. 11. SEM photos showing the difference of pore orientation of the samples with the same final density of 80% by hot forging under 100 N load starting from (a) 75% density and (b) 65% density. Before these two starting densities, the samples were freely sintered.

at identical density can be achieved using discontinuous hot forging.

Another aspect about the microstructure is the pore structure, which has been specially discussed elsewhere [39]. In hot forged samples, pores are elongated along the loading direction because the externally applied axial compressive load promotes the growth of necks, which have their normal parallel to the loading direction. Those oriented pores have been shown to cause anisotropic sintering behaviour during hot forging [39]. Using discontinuous hot forging, preferred pore orientation along the loading direction can be reduced. This is visualised in Fig. 11, where two samples with a final density of 80% are compared, which were hot forged under 100 N load starting from 75% (sample A) and 65% (sample B) density, respectively. Pores in sample A are still randomly distributed without any observable orientation, like completely free sintered samples, although the sample A was acted on by a compressive load during sintering. On the contrary, pores in sample B are mostly elongated along the z-axis, as reported previously [39]. The comparison indicates that pores remain isotropic in discontinuously hot forged samples, at least within the density range of 5% right after a uniaxial compressive load was applied.

In addition, Fig. 12(a),(b) provide quantitative evidence that discontinuously hot forged samples remain isotropic within a certain density range after a uniaxial was applied. As a 100 N uniaxial compressive load was applied from 65% density up to 80% density, the sample presented anisotropic free sintering behaviour after 80% density

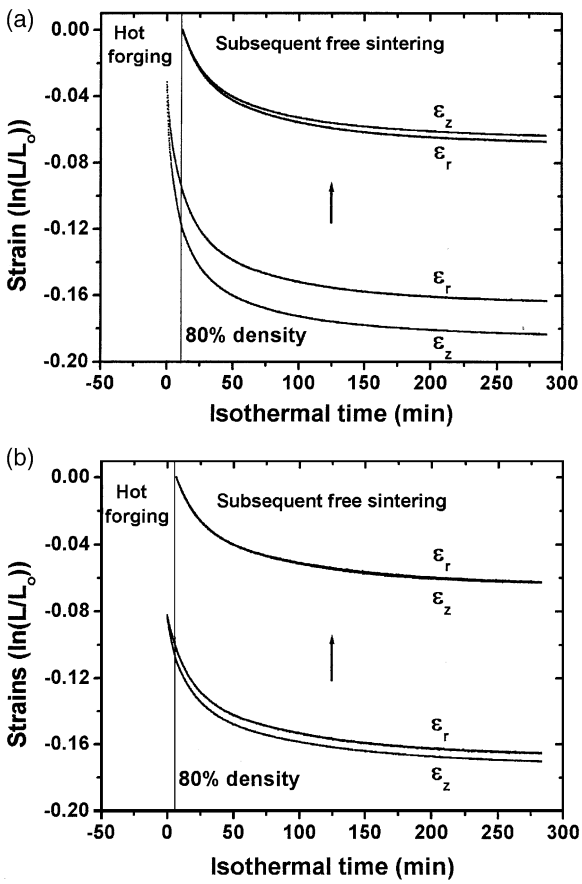

Fig. 12. Sintering strains of samples which were first hot forged under 100 N uniaxial compressive load applied from (a) the onset of isothermal sintering (about 65% density) and (b) 75% density (before this density, the sample was freely sintered), respectively, up to 80% density, and then freely sintered after 80% density by rapidly releasing the uniaxial load. For free sintering, the strains were shifted to zero by considering the dimensions of the sample at 80% density as original dimensions.

which is characteristic of larger radial strain than axial strain found in hot forged samples [39]. In contrast, if the same load was applied from higher density (75% density) up to 80% density, then the radial strain remains equal to the axial strain during subsequent free sintering.

5. Discussion

The results in this study have shown that an anisotropic microstructure (Fig. 11) and reduced grain growth (Fig. 10) develop during hot forging. As discussed previously [39], this invalidates the stress analysis based on the viscoelastic analogue using density as sole microstructural variable.

In contrast, the application of discontinuous hot forging assures the validity of the microstructural assumptions. Although in some studies [18,26,27] the strain rates were corrected for grain growth, preferred pore orientation was not considered. Moreover, the grain size measurement for low-density samples is difficult and the effect of grain size on strain rates mainly relies on theoretical prediction. In this study, the as-measured real strain data were directly used in the calculation and the influence of the microstructure was eliminated by the discontinuous hot forging technique. Therefore, sintering parameters as determined in this study are isotropic and have included the effect of grain growth.

Results in Figs. 5 and 6 demonstrate the value of the discontinuous hot forging technique. The developing anisotropy has lead to a difference in the sintering stress and uniaxial viscosity. In Fig. 5, at a fixed density (for example, 85%), elongated pores along the loading direction (z-axis) cause the component of the sintering stress tensor in z-axis to decrease by about a factor of 2, so that a smaller externally applied tensile stress can stop the axial shrinkage. This influence is mitigated by the effect, that after long hot forging times the grain size is reduced (Fig. 9), which contributes to an increase in sintering stress. Therefore, elongated pores in z-axis and reduced grain size at an identical density caused by uniaxial loads will prompt a smaller sintering stress. This is generally predicted to occur in the experimental determination of sintering parameters by conventional (continuous) hot forging.

The sintering stress determined above (Fig. 7) shows a consistent tendency with theoretical predictions [12,13]. When grain growth is taken into account in the models, sintering stress increases slightly with density and then decreases at higher density. The intrinsic sintering stress Σ can be expressed theoretically in terms of curvature and interfacial energy, as shown in the most basic form in Eq. (6) [24].

$$\Sigma = \frac{2\gamma_b}{G} + \frac{2\gamma_s}{r} \quad (6)$$

where γ_s and γ_b are surface energy and grain boundary energy, G and r are grain size and radius of curvature of pores. At low density pores play the dominant role in the sintering stress and affect an increase in sintering stress with density because smaller pores imply a larger surface curvature. At higher density most pores are closed and decrease in number due to pore coalescence but the grains coarsen with time (Fig. 9) so that the sintering stress decreases with density. Fig. 7 compares the measured sintering stress σ_s with Riedel's model (b.c.c particle packing, 3D2 open pores) [12] using a constant ν_p of 0.333 and including grain growth (Fig. 9), considering that the uniaxial sintering stress σ_s equals the hydrostatic sintering stress Σ multiplied by $(1-2\nu_p)$. The results indicate a semi-quantitative agreement.

The discussion on the uniaxial viscosity follows similar arguments. The effect of loading treatment on the viscosity can be clearly seen in Fig. 6, which shows differences in viscosity by up to a factor of four at a density of 95%. Compared to Fig. 5, uniaxial viscosity at a lower density is insensitive to hot forging processing; at higher density, however, it presents a stronger dependence so that hot forging makes a clear difference. A reduction of grain growth during extended hot forging will lower the uniaxial viscosity. On the other hand, this effect is mitigated as elongated pores along the loading direction cause a higher density distribution in the z-axis, thereby contributing to an increase in the uniaxial viscosity. Therefore, in Fig. 6, the sample with 95% density prepared by hot forging from 65% density will have more oriented pores and smaller grain size than the sample with the same density obtained by hot forging from 85% density. In the case of the influence of extended hot forging times on uniaxial viscosity, the influence derived from the reduced grain size overrides the influence stemming from the anisotropy, presumably since the viscosity is very sensitive to grain size (power of 3 for grain boundary diffusion).

The measured sintering viscosity E_p at lower density slightly increases with density and then has a stronger dependence on density after about 85% density. Particularly, at the final stage of sintering, grain coarsening greatly contributes to an increase in viscosity. The viscosity of a porous sintering body is related to grain size [17–20] specifically, it is proporational to the power of 2 or 3 of grain size [18,19], depending on prevalent diffusion mechanism. Thus, the grain size measured in this study (Fig. 9) was used in these theoretical models. Moreover, for sake of comparison, the uniaxial viscosity E_p is normalised by its value at the onset of sintering where the relative density of the sample is 65% in order to eliminate the effect of different initial grain sizes and sintering temperatures used in these models. We then define

$$\overline{E}_p = \frac{E_p(\overline{\rho})}{E_p(0.65)}. \quad (7)$$

Plots for several available models and measured viscosities using Eq. (7) are compared in Fig. 13. Those models predicted rather similar functions at low density, but a different dependence at high density. Among them, Rahaman's model provides a good prediction over the whole density regime. Since the effect of grain size was not built in, Scherer's and Skorokhod's models predicted a rather low uniaxial viscosity. Scherer's model was developed for viscous materials.

Although the sintering stress is a fundamental parameter in the understanding of the sintering pro-

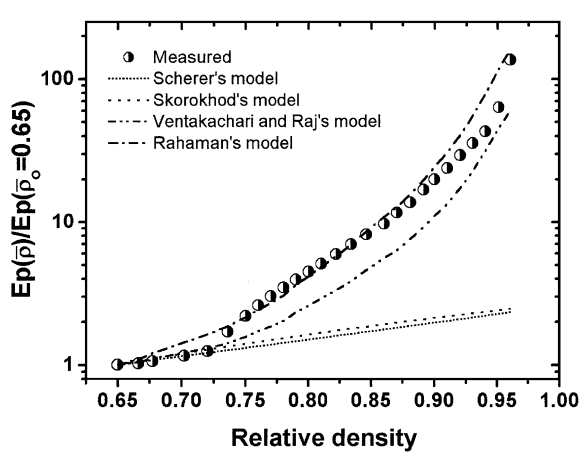

Fig. 13. Comparison of the measured and theoretically predicted uniaxial viscosities. All viscosities have been normalised by the viscosity at the onset of sintering ($\overline{\rho}_o = 0.65$).

cess, the uniaxial sintering viscosity E_p is a very important sintering parameter together with the viscous Poisson's coefficient ν_p, both of which are used to obtain other sintering parameters, for example, bulk viscosity $K_p = \frac{E_p}{3(1-2\nu_p)}$ and shear viscosity $G_p = \frac{E_p}{2(1+\nu_p)}$, or to describe constrained sintering problems. Further experimental work therefore is geared to evaluate the evolution of the viscous Poisson's coefficient as a function of density.

6. Conclusions

1. An improved hot forging technique, i.e. discontinuous hot forging was described and for the first time applied successfully for the experimental determination of the sintering stress and the uniaxial viscosity.
2. Implied assumptions, such as isotropic and identical microstructures between free sintered and hot forged samples, were strictly taken into account in the analysis, and well satisfied through discontinuous loading experiments.
3. Oriented pores and smaller grain size caused by uniaxial compressive loads, as compared to free sintered samples, in combination have brought about the determination of smaller sintering stress and uniaxial viscosity in conventional hot forging experiments.
4. The uniaxial sintering stress is shown to increase in absolute value up to a density of about 80–85% and then decrease again. The uniaxial viscosity increases slightly at low density (less than 85%) and then indicates a stronger dependence on density.

Acknowledgements

This work was financed by the Deutsche Forschungsgemeinschaft (DFG) under contract number Ro 954/14.

References

[1] Christensen RM. Theory of viscoelasticity, an introduction, 2nd edn. New York: Academic Press, 1982.
[2] Scherer GW, Simon SM. J Am Ceram Soc 1982;65:352.
[3] Riedel H, Meyer D, Svoboda J, Zipse H. Int J Refr Met Hard Mat 1993-94;12:55.
[4] Lu G, Sutterlin RC, Gupta TK. J Am Ceram Soc 1993;76:1907.
[5] Kanters J, Eisele U, Rödel J. J Am Ceram Soc 2001;84:2757.
[6] Bordia RK, Raj R. J Am Ceram Soc 1985;68:287.
[7] Scherer GW, Garino T. J Am Ceram Soc 1985;68(4):216.
[8] Stech M, Reynders PR, Rödel J. J Am Ceram Soc 2000;83:1889.
[9] De Jonghe LC, Rahaman MN. J Am Ceram Soc 1984;67:C214.
[10] Skorohod V, Olevsky E, Shtern M. J Sci Sint 1991;23:79.
[11] McMeeking RM, Kuhn LT. Acta Metall 1992;40:961.
[12] Svoboda J, Riedel H, Zipse H. Acta Metall 1994;42:435.
[13] Riedel H, Svoboda J, Zipse H. Acta Metall 1994;42:445.
[14] Parhami F, McMeeking RM. Mech Mat 1998;27:111.
[15] Olevsky EA. Mater Sci Eng 1998;R23(2):41.
[16] Scherer GW. J Non-Cryst Solids 1979;34:39.
[17] Raj R, Bordia RK. Acta Metall 1984;32:1003.
[18] Venkatachari KR, Raj R. J Am Ceram Soc 1986;69:499.
[19] Rahaman MN, De Jonghe LC, Brook RJ. J Am Ceram Soc 1986;69:53.
[20] Hsueh CH, Evans AG, Cannon RM. Acta Metall 1986;34:927.
[21] Dawihl W, Rix W. Z Metallkunde 1949;40:115.
[22] Aigeltinger EH. Int J Powder Metall Powder Tech 1975;11(3):195.
[23] De Jonghe LC, Rahaman MN. Acta Metall 1988;36(1):223.
[24] Raj R. J Am Ceram Soc 1987;70(9):C210.
[25] Gregg RA, Rhines FN. Metall Trans 1973;4(5):1365.
[26] Rahaman MN, De Jonghe LC. J Mater Sci 1987;22:4326.
[27] Cheng T, Raj R. J Am Ceram Soc 1988;71(4):276.
[28] De Jonghe LC, Rahaman MN. Rev Sci Instrum 1984;55:2007.
[29] Scherer GW. J Am Ceram Soc 1986;69:C206.
[30] Geguzin Y, Matsokin V, Pluzhnikova D, Dayad H. Sov Powd Met 1986;2:39.
[31] Panda PC, Wang J, Raj R. J Am Ceram Soc 1988;71(12):C507.
[32] Cai PZ, Messing GL, Green DL. J Am Ceram Soc 1997;82(2):445.
[33] Salamone SM, Stearns LC, Bordia RK, Harmer MP. J Am Ceram Soc 2003;86(6):883.
[34] Bordia RK, Scherer GW. Acta Metall 1988;36:2393.
[35] Bordia RK, Scherer GW. Acta Metall 1988;368(9):2399.
[36] Rahaman MN, De Jonghe LC, Hsueh CH. J Am Ceram Soc 1986;69(1):58.
[37] Raj R. J Am Ceram Soc 1982;65(3):C46.
[38] Mikeska KR, Scherer GW, Bordia RK. Ceram Trans 1990;7:200.

[39] Zuo R, Aulbach E, Bordia RK, Rödel J. J Am Ceram Soc 2003 (in press).
[40] Rahaman MN, De Jonghe LC. J Am Ceram Soc 1984;67(10):C205.
[41] Aulbach E, Zuo R, Rödel J. Exp Mech 2003 (in press).
[42] Kanters J, Eisele U, Böder H, Rödel J. Adv Eng Mat 2001;3(3):158.